Liquid film formation: prediction accuracy of different numerical approaches

Liquid film formation: prediction accuracy of different numerical approaches

Giuliano Agati[1], Adriano Evangelisti[1], Serena Gabriele[2], Franco Rispoli[1], Paolo Venturini[1] and Domenico Borello[1]

[1]Sapienza Università di Roma, Dipartimento di Ingegneria Meccanica e Aerospaziale, via Eudossiana 18, 00184, Roma (Italy)

[2]Baker Hughes, Viale F. Matteucci, 2, Florence, Italy

giuliano.agati@uniroma1.it

Abstract. In counteracting fouling phenomenon in gas turbines, which leads to system inefficiencies and performance degradation, water washing technique is very often adopted. Water droplets sprays are injected and, hitting the solid surfaces, remove the dirt deposition. Among the collateral undesirable phenomena related to water washing, blades erosion and liquid film formation are the most remarkable. Despite the former issue was extensively assessed by the authors in previous works, up to the authors' knowledge the risk of liquid film formation due to water washing was scarcely investigated. Liquid film formation and spreading on a solid surface is a complex phenomenon involving a large number of physical events, such as: droplets impact on a solid surface, splashing phenomena, liquid film dragging under the effect of the carrier phase and droplets separation from the film in proximity of geometry discontinuities. In this paper, an extensively used experimental test case involving all these phenomena was used to test different numerical wall film models available in literature. The test case consists in the injection of a liquid jet in a high velocity crossflow. Some of the liquid jet mass impacts on the opposite solid surface generating a wall film which develops under the dragging effect of the crossflow. A Lagrangian approach was used to track the suspended droplets within the flow field by also considering the turbulent dispersion by means of a Random Walk model. Droplets-wall interaction is considered according to the Stanton-Rutland model, which provides the outcome of a collision (deposit, rebound or splashing), depending on the local impact conditions. If a droplet sticks on a solid boundary, a liquid film generates. Droplets atomization is also accounted for by using the Madabhushi model while Friederich separation model was selected to take into account the detachment of droplets from the film at the geometry edge. Three different numerical simulations have been performed based on different approaches used to solve the liquid film evolution, namely Eulerian one-way coupling, Eulerian two-way coupling and Lagrangian two-way coupling. Numerical results have been compared with the experimental ones from both a qualitative and a quantitative point of view. The wall film shape, its spatial distribution and the variation of the film thickness of the wall centreline have been compared between experimental and numerical simulations proving that the Lagrangian 2-way coupling approach better reproduces the liquid film dynamics observed in the experiments.

1. Introduction

Although the ongoing necessary push towards a decarbonisation of energy production processes [1], gas turbine engines will still play a crucial role in the next years because of their elasticity, compactness, and relatively high efficiency. In stationary applications they are always equipped with filtering systems aiming at removing solid particles (i.e., dust, sand, dirt, etc.) from the air flow sucked by the engine. However, there is always a number of particles escaping the filters and reaching the compressor where they might deposit, leading to airfoil geometry variation and to aerodynamic losses. It was estimated that most of the performance losses of gas turbine engines can be ascribed to compressor issues, with fouling being one of the major ones ([2],[3]). Nevertheless, compressor efficiency losses due to fouling can be partially recovered during the machine life without the need of replacing any of its parts ([2], [4]). On-line and off-line water washing techniques [4]-[7] are in fact nowadays commonly used, with the former becoming more and more interesting because it permits to increase the time interval between two off-line washings for which a shut-down of the plant is needed [8]. Accordingly, in the last years an increasing number of publications are focusing the attention on on-line washing. Dominizi *et al*. [9] performed a Life Cycle Assessment study demonstrating the feasibility of on-line washing despite the duties related to freshwater availability, heating and pumping. The effect of droplet size on compressor water washing efficiency is studied in Abgadede *et al*. [10]. The authors conclude that larger droplets lead to a better recovery of power losses due to compressor fouling. The effect of the detergent used for compressor washing was the focus in Baikov *et al*. [11]. A parametric study of an online aero engine washing system was performed in [12], varying the inlet pressure and size of droplets. To optimize the water injection system, Wang *et al*. [13], analysed the effect of slope angle of the compressor wall on the splash condition of washing droplets. Igie *et al.* [14] investigated the impact of off-line and on-line compressor washing by analysing machine-generated data of four different gas turbine plants. In [15] the economic viability of the online washing process of axial compressors is estimated, finding that larger engines have a higher return on investment in comparison to the smaller units. However, since on-line water washing is performed with the engine working at (or close to) its nominal speed [16], the high speed impingement of water droplets with the compressor blades may lead to the erosion of the blades ([7], [17]). Aiming at simulating the washing process and erosion due to water washing systems, the authors of the present paper developed first a water droplets erosion model [18] and then an algorithm to perform long-term predictions of the washing efficiency and of the erosion risk ([19]-[22]).

Another shortcoming associated to water washing systems is the liquid film formation on the machine surfaces. From low energy droplets impacts, the dispersed phase tends to stick on the machine surfaces forming a liquid film. Under the drag action of a gaseous carrier phase, the liquid film evolves, depending on the momentum impressed and the wall friction action. In the case of water washing, as the liquid enters the rotor region, in the form of both a wall film and nebulized droplets, a strong centrifugal force tends to push it toward the rotor case. This can lead to the formation of a liquid film on the rotor case which might interfere with the blade tips, eventually provoking severe damages. In this framework, it is crucial to improve our understanding on the behaviour of liquid film formation due to dispersed droplets impact. In fact, on the one hand, it is necessary to minimize the amount of water sprayed to reduce the risk of erosion and liquid film formation; on the other hand, the injected water mass must be enough to properly wash the blades.

The fate of a fine spatially distributed liquid phase, injected in a gaseous control volume was deeply investigated over the past years. The growing interest in investigating the possible liquid film onset has its root in the optimization of the diesel engines design. This is the case of the pioneering work carried out by Kim *et al*. [23] where a spray impingement and the liquid film formation were modelled inside high-speed direct injection diesel engines. They demonstrated a higher tangential velocity of the piston bowl reduces the liquid accumulation, lowering, in turn, the film development. In [24], also the relative low temperature wall surfaces effect on the wall film formation was taken into account and models for droplet-droplet, droplets-film impacts and film breakup were developed. Improvements in the wall film modelling are brought by O' Rourke *et al.* [25]: they extended the CFD model adopted in [24] by assessing the wall film formation in port-injected engines, including also the impingement-pressure

spreading and fluid motion due to inertia forces, with particular attention in modelling the liquid expulsion from valve seat areas when valves close. Wall film development is also important for lubrication purposes. This is the case analysed by Singh *et al.* [26], in which the fluid movement is assessed through the employment of an Eulerian approach. The particular viscous behaviour of such an oil involves the study of the shear stress term by introducing and investigating a dynamic contact angle, needed to account for the film attachment on the sliding plane. Shear stress conditions were proved to cause rivulets propagation due to contact angle between wall and liquid sheet, as descripted by Meredith *et al.* [31].
The work developed by Shedd *et al.* [27] work is focused on the experimental quantification of the wall film formation on a flat surface by considering a shear-driven liquid film displacement due to a cross-flow air flux. Three different atomization phenomena are taken into account, i.e., droplets splashing, film surface atomization (stripping) and film breakup at the trailing edge of the channel. Phenomena as first liquid column breakup and droplet-film interaction are also considered and visualized by the elaborated photograms. The aforementioned experimental work was chosen as a test case to validate numerical modelling approaches in several papers, because of the quantity of interesting physical phenomena involved. For example, in [28] a model able to describe the evolution of the interface between the liquid and the gas phase was developed. After atomization takes place, droplets are generated and tracked with a Lagrangian approach. Shear stripping, turbulent column break-up, splashing and film separation were taken into account with good results when compared with the reference measurements of the film thickness along the target surface. In [29], the test case was used to validate the Eulerian thin film model (ETFM) implemented in Ansys Fluent. Convergence stability issues were found when activating the gas-film momentum coupling, the separation and the surface tension action on the wall film. In [30] the authors skipped this problem by implementing the same approach in OpenFoam finding a good agreement with the experimental results. Wall film is also affected by geometrical structure of the sliding plane and aerodynamic instabilities, taken into account through the definition of a critical angle and a film Weber number, respectively; for this reason, a separation criterion, as proposed by Friederich *et al.* [32], is needed to enable the liquid fluid vane detachment in approaching a more physical description in proximity of solid structure trailing edges, as at the end of a rotor blade.
All the aforementioned papers base the analysis of the wall film formation and movement on the ETFM. Lately, a particle-based Lagrangian approach has been added in Ansys Fluent formulated on the theory developed in [33]. The impinging liquid jet test case developed by Shedd *et al.* [27] is also here chosen to select and validate the best modelling strategy to assess the wall film formation in axial compressors subject to online water washing techniques.

2. Models and governing equations

The two-phase flow is here numerically assessed by using an Eulerian-Lagrangian approach. In this chapter details regarding the turbulent field modelling and the equation solved for the dispersed phase tracking are provided. Two different approaches are available in the open literature to study the development and the dynamics of a thin liquid film on a surface. The Lagrangian wall film model threats the film as single liquid parcels and tracks their trajectories on the solid surfaces integrating the particle equations under proper forces. It is therefore well suited for fast transient effects. Besides this, the Eulerian wall film model is more appropriate for steady wall films [34]. The last part of this chapter compares equations for the wall film in the two different approaches, highlighting similarities and differences.

2.1 Carrier phase

Turbulence of the carrier phase is modelled by solving Unsteady Reynolds Averaged Navier-Stokes (U-RANS) equations and employing the well-established, widely accepted k-ε Realizable model [34]. Near the walls, and enhanced wall treatment is adopted. In this approach, the whole domain is subdivided into a viscosity-affected region and a fully-turbulent region, and two different approaches (the two-layer model and enhanced wall functions) are combined. The blending of the two regions is determined by a wall-distance-based, turbulent, Reynolds number. The governing equations are solved using the coupled Pressure-Based solver algorithm. The SIMPLEC solution method was selected for the pressure-velocity

coupling. Pressure is discretized spatially by the second order upwind scheme, while for all the other variables a first order scheme is adopted. The time advancement is performed by using a first order implicit method.

2.2 Dispersed phase

Droplets tracking relies on the discrete phase model (DPM) implemented in Ansys Fluent [34]. The software predicts the trajectory of the dispersed phase by integrating the force balance on the particle in a Lagrangian framework. The force balance equates the particle inertia with the forces acting on the particle, where the drag force plays a dominant role. Both one-way and two-way coupling approaches are tested in this work. A random Random Walk Model is also activated in all the performed simulations to account for the turbulence effect on the droplets dispersion. For this purpose, the eddy lifetime (τ_e) is calculated as a function of the fluid Lagrangian integral time T_L [34]. Droplets are continuously injected after a converged solution is reaches for the carrier phase. The injection is realized by using the solid cone injector implemented in Ansys Fluent and the droplets are tracked until all of them reach their final destination, i.e. either they exit the domain or they impact the target surface.

The injected liquid phase leads to the onset of several phenomena as primary and secondary atomization (or breakup) and the impact on the solid surface. If the impacted droplet deposits on the wall, a liquid wall film is generated. At the geometry edges, wall film separation phenomena might occur and droplets are re-suspended in the flow. The major considered physical phenomena acting on the injected liquid phase are summarized in Figure 1.

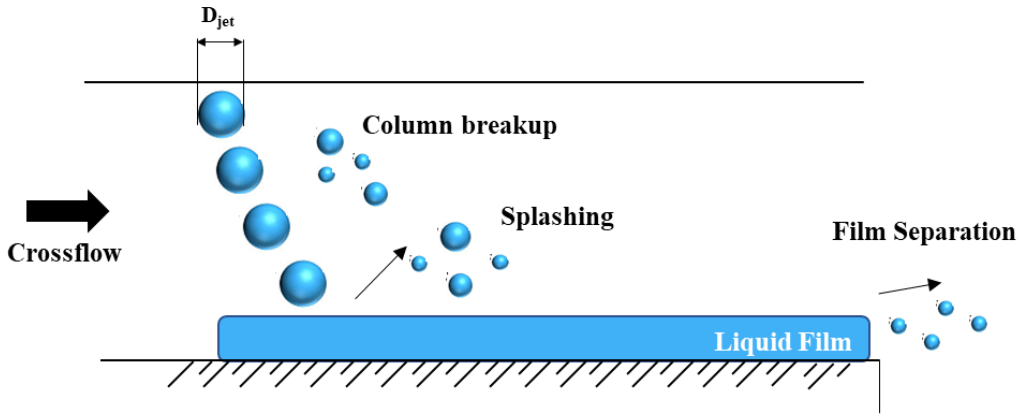

Figure 1: Major physical phenomena acting on liquid column jet considered in the present work.

Indeed, the wall film formation depends on the quantity of liquid mass depositing on the target surface. Droplets impact on a solid surface is an extremely complex phenomenon and its physical behaviour is strongly affected by the impact conditions. In the present work, the Stanton-Rutland model [36], extended using the concepts from O'Rourke and Amsden [25], is adopted to predict the outcome of a droplet impact on a wall. In this model, four different impact regimes are considered for a drop-wall interaction according to local impact conditions (i.e., local wall temperature and a parameter *E* linked to the impact velocity). The possible regimes are: deposition, spreading, rebound and splash. In fact, for low impact velocity values, it was observed that the drop sticks to the wall but as impact energy increases, a lamella forms which spreads and recoils until all the energy is dissipated. For higher velocity magnitudes, if the spread energy dissipations reduce, lamella reaches its maximum extent with a significant energy of retraction and rebound may also occur. This feature was observed only on highly non-wettable surfaces. For moderate impact velocities, the rim of the lamella may destabilize in the spreading phase and form regular structures called fingers. If surface tension is not strong enough to maintain cohesion of the retracting lamella, a break-up event may eventually be triggered. In the highest impact velocity range, splash occurs: the prompt splash is characterised by tiny droplets detached at the periphery of the liquid lamella generated by the spreading drop; as surface tension is reduced, high temperature

environments, the liquid lamella can detach from the wall, resulting in the so-called corona splash scenario.
The quantity of mass collecting on the film depends also on the droplets breakup. In order to evaluate the occurrence of this phenomenon on the injected liquid flow rate, the Madabhushi model was selected. In fact, this model considers both primary breakup (accounted for are by using the Wave model [37]), and the effects of secondary breakup due to turbulence, capillary and aerodynamic forces through the model suggested by Pilch and Erdman [38]. Madabhushi model was selected since it is suitable for numerical simulations of a liquid jet in a subsonic crossflow [34].
Moreover, separation of liquid wall film might occur at the domain edges because of geometrical discontinuity in the film deployment; the instability effect is estimated trough the employment of a wall film separation model based upon the assumption of Friederich et al. [32]. The model considers that separation of liquid wall film occurs in presence of a corner when the inertial force overcomes the surface tension and the weight contributions. Two main conditions are requested in order to take into account a film breakup at the trailing edge: a critical Weber number has to be overcome, and the geometrical angle has to be larger than a critical value θ_{crit}. Based on analytical and physical assumptions, in the present paper values of 2 and 15° were selected for We_{crit} and θ_{crit}, respectively.

2.3 Wall Film
The Wall film evolution is analyzed carrying out two different modelling approaches; the Eulerian framework is compared with the Lagrangian one in order to point out the main computational differences. The first method describes the unit surface momentum balance as shown in eq. 1:

$$\frac{d}{dt}\left(\rho_l h\vec{v}_l\right) = -\left(\vec{\nabla}_s\cdot\left(\rho_l h\vec{v}_l\right)\right)\vec{v}_l - \vec{\nabla}_s\cdot\bar{\bar{D}}_V - h\vec{\nabla}_s p_L + \rho_l h\vec{g}_\tau + \frac{3}{2}\vec{\tau}_{fs} - 3\frac{\mu_l}{h}\vec{v}_l + \dot{\vec{q}}_s + \vec{\tau}(\theta_w) \tag{1}$$

On the left-hand side the material derivative of the wall film is isolated, while on the right-hand side it is possible to recognize part of the convective term related to the film momentum, the advective tensor term depending upon the quadratic film velocity representation and the pressure gradient, including the effects of the gas flow pressure, gravity normal component to the sliding plane and surface tension action:

$$\begin{aligned} p_L &= p_{gas} + p(h) + p(\sigma) \\ p(h) &= -\rho_l h(\hat{n}\cdot\vec{g}) \\ p(\sigma) &= -\sigma\vec{\nabla}_s\cdot\vec{\nabla}_s h \end{aligned} \tag{2}$$

The fourth term, instead, represents the parallel sliding-direction acceleration component due to gravity, while fifth and sixth terms represent the shear stresses exerted on the gas-film and film-wall surface interfaces, respectively. The seventh term is representative of the momentum source due to droplet collection or separation and, the last one is the contact angle stress fundamental to match the partial wetting properties of the sliding surface for considering the rivulets formation, as also stated by Meredith *et al.* [31]:

$$\vec{\tau}(\theta_w) = \beta\sigma(1-\cos\theta_w)\vec{\nabla}_s w \tag{3}$$

The other interpretation is based on the Lagrangian modelling of the liquid film [33] and reads:

$$\rho_l h\frac{d\vec{u}_p}{dt} = -\tau_g\hat{t} + \vec{\tau}_w + \vec{F} + \rho_l h(\vec{g} - \vec{\alpha}_w) \tag{4}$$

The material temporal variation of the film particle velocity related to its inertia is equal to a sum of different forces. The first term on the right-hand side of eq. (4) represents the shear-driven stress due to the drag action of the gas phase at the interface with the liquid film; it is projected on the tangential direction, in order to guarantee the film motion. The second term is the shear stress due to the friction force the sliding surface imposes to the liquid film; it accounts for the relative velocity difference between film particles and wall surface and its expression is defined by:

$$\vec{\tau}_w = -\frac{2\mu_l}{h}\left(\vec{u}_p - \vec{u}_w\right) \tag{5}$$

The penultimate term in eq. (4) is the unit area force needed to keep the liquid film attached on the sliding surface; the last one represents the body force acting on the unit film particle.
Despite the Eulerian model offers a more detailed description of the film evolution, allowing for example the consideration of the contact angle film action for partially wet surfaces, with the Lagrangian approach the wall stress term takes explicitly into account the possible walls rotation and it results more appropriate to model fast transient liquid film cases.

3. Computational details

The geometry used in the performed simulations corresponds to the experimental rig described in [27] and it is shown in Figure 2 together with a 2D representation of the computational mesh. The domain is composed of a 120 mm long expansion duct. In comparison with the reference paper, the length L_2 was increased to make the simulations not dependent on the outlet boundary condition. The length of the impinging plate where the wall film is monitored (L_1) is equal to 40 mm, while the width of the duct was slightly decreased with respect to the reference paper to reduce the simulations computational cost. The main domain dimensions are reported in Table 1. Structured hexahedral symmetric mesh is used because of the uniformity of the geometry, with a total number of 2.8 M cells properly clustered near the walls. Different clustering parameters have been tested in such a way to meet the *y*+ requirements of the adopted near wall turbulence treatment.

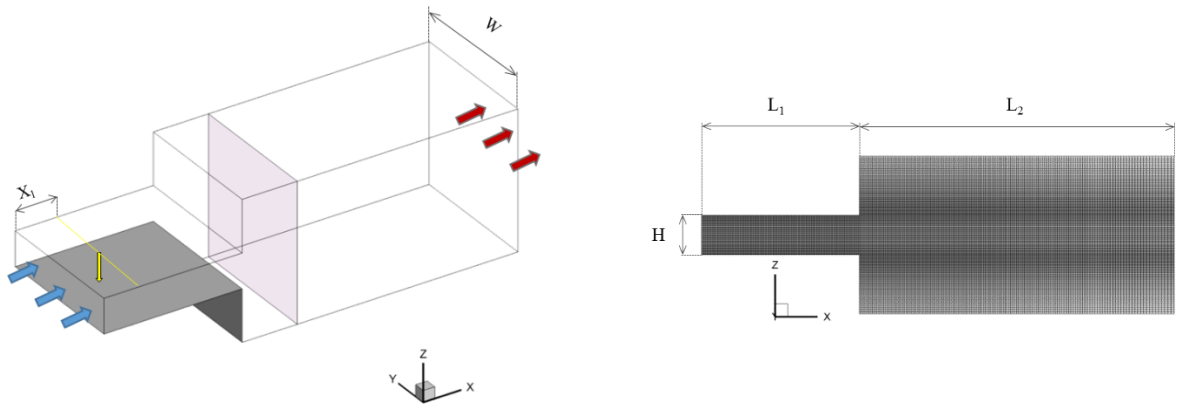

Figure 2: Computational domain (left) and mesh (right) used in the performed simulations. Blue and red arrows represent the fluid flow inlet and outlet boundary conditions, the yellow vertical arrow shows the position of the injection point.

At the crossflow inlet (blue arrows in Figure 2-left) a velocity of 81 m/s is imposed, while a pressure boundary condition is adopted for the outlet where the atmospheric pressure is set. All the walls are treated as adiabatic no-slip walls, and periodic boundary conditions are applied on the lateral surfaces. Droplets are continuously injected on the centreline by adopting a solid cone injection model at a distance X_1=10 mm from the domain inlet (downward arrow in Figure 2-left). As prescribed in the

Madabhushi model [34], the liquid jet is represented by a liquid column of spherical droplets of equal diameters $D_p = D_{jet}$, being the latter the nozzle diameter. Droplets injection velocity (12.7 m/s) is computed according to the liquid mass flow rate and the nozzle diameter. The resulting injection droplets aerodynamic number is equal to 195, while the jet-to-crossflow momentum-flux ratio (q) is 13.5. When the droplets impact the lower wall the Stanton-Rutland model is activated as explained in Section 2. If the droplets stick to the lower wall, they form a liquid film which can separate from the plane edge or slip on the vertical lower wall of the expansion duct. Because of the large number of the dispersed parcels in the field and the high computational cost needed to track them, the dispersed phase outlet boundary conditions (pink surface in Figure 2-left) was shifted backward with respect to the carrier phase outlet BC. In this way the computational cost was reduced not altering the phenomena under analysis. The main geometrical parameters and the adopted boundary conditions are summarized in Table 1.

Table 1: Geometrical details and boundary conditions for the considered set of simulations.

Nozzle Diameter [mm]	0.5
Injection Point (X_1) [mm]	10.0
L_1 [mm]	40.0
L_2 [mm]	80.0
W [mm]	40.0
Liquid Mass Flow Rate [kg/s]	1.95×10^{-3}
Jet Velocity [m/s]	12.7
Crossflow Velocity [m/s]	81.0
Outlet Pressure [kPa]	101.325

The time advancement assumes a different timestep depending on the approach used to study the wall film development. In fact, due to numerical instabilities, in the Eulerian simulations an inferior timestep has been adopted in comparison with the Lagrangian one. All the simulations are initialized with the same converged steady flow field where residuals threshold values are set equal to 1.0E-5. The integration of droplets motion is achieved by an automated tracking scheme that permits switching between a numerically stable implicit low order scheme and a trapezoidal higher order one.
A set of three different simulations is here assessed. The Eulerian wall film model is tested in both a 1-way and 2-way coupling framework. The analyzed Lagrangian wall film model necessarily assumes a 2-way coupling approach. When the mutual interaction between the carrier and the disperse phase is considered, the number of iterations per timestep is large enough to guarantee that a converged fluid flow solution is always reached. Numerical details about the performed simulations are reported in Table 2.

Table 2: Set of performed simulations with the most relevant numerical details.

Case	Film Approach	2 Phases Coupling	Acronym	Simulation Timestep
1	Eulerian	1-way coupling	EWF-1way	5.0E-6 s
2	Eulerian	2-way coupling	EWF-2way	5.0E-6 s
3	Lagrangian	2-way coupling	LWF-2way	3.0E-5 s

4. Results and discussion

As reported in Section 3, a comparison of the results obtained using EWF-1way, EWF-2way and LWF-2way approaches is performed with respect to the experimental data reported in [27] and [28]. Formation and evolution of a liquid film on a solid surface is a complex unsteady process. Therefore, a statistical analysis is performed to compare the numerical results with the experiments. Statistics are sampled for a different number of timesteps, depending on the time each simulation needs to reach a steady state condition. For this reason, as also suggested in [29], results are analysed from the moment the time variation of the liquid film mass deposited on the target surface fell below 3%. As illustrated in Figure 3, in EWF simulations (Figure 3-left) a smaller time interval was needed to reach a steady condition with respect to LWF simulation (Figure 3-right). It is also worth noticing that, while the steady wall film mass in the LWF-2way is similar to that in EWF-2way, in EWF-1way it is an order of magnitude smaller. This can be ascribed to the effect of two-phases coupling approach. Indeed, as shown in Figure 4, since in the 1-way coupling based simulations the flow field is not altered by the liquid phase, jet impinges the bottom wall at a larger distance from the injection projection (point A in figure) in comparison with the simulations in which the 2-way coupling approach was implemented. In the latter cases, the carrier phase interacts with the liquid jet thus reducing its streamwise velocity in the duct central region. Moreover, in the 1-way coupling case, the undisturbed flow velocity results in a stronger liquid column atomization. Both these effects result in a smaller amount of water hitting the wall in the 1-way phase coupling simulation.

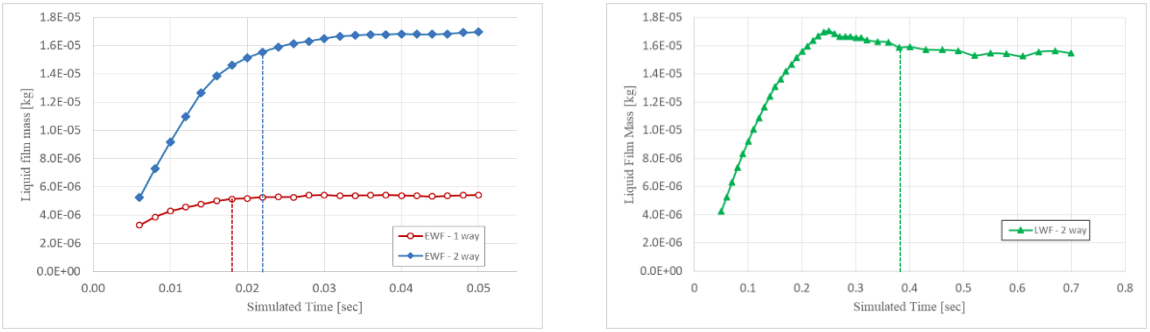

Figure 3: Time evolution of liquid wall film mass in EWF (left) and LWF (right) approaches.

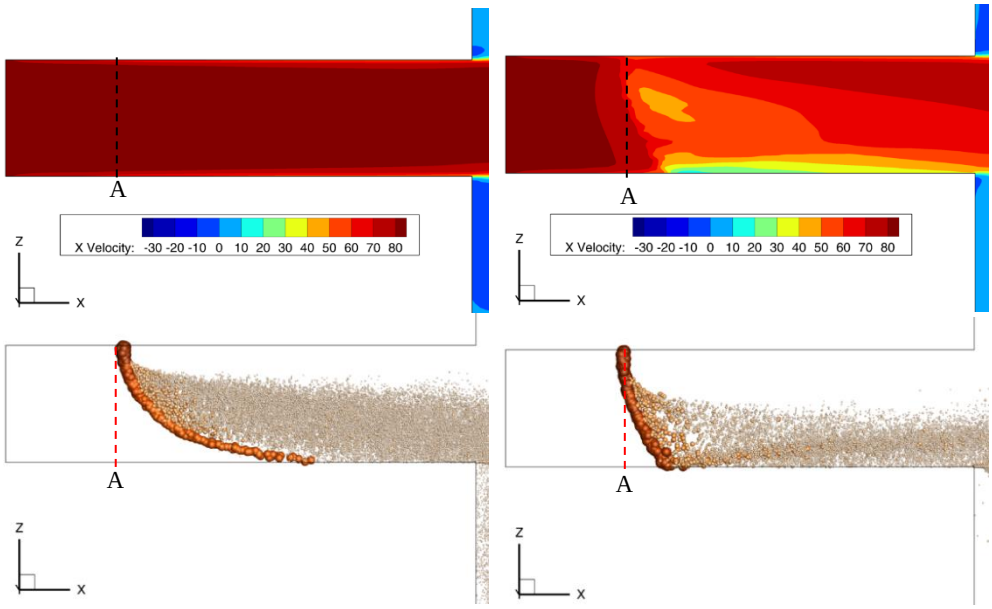

Figure 4: Lateral (x-z plane) view of the flow filed (top) and water jet (bottom) in EWF-1way (left) and EWF-2way (right) approaches.

Beside the liquid film mass, also the maximum film thickness is monitored to evaluate the starting of the steady state condition. The plots are not reported for the sake of brevity. While for EWF simulations the maximum film thickness reached a semi-steady state in correspondence with the deposited mass (Figure 3-left), for the LWF simulation this quantity strongly oscillates until a simulation time t = 0.38 s is reached, then it stabilizes. Therefore, in the present study LWF-2way statistics were sampled from that time.

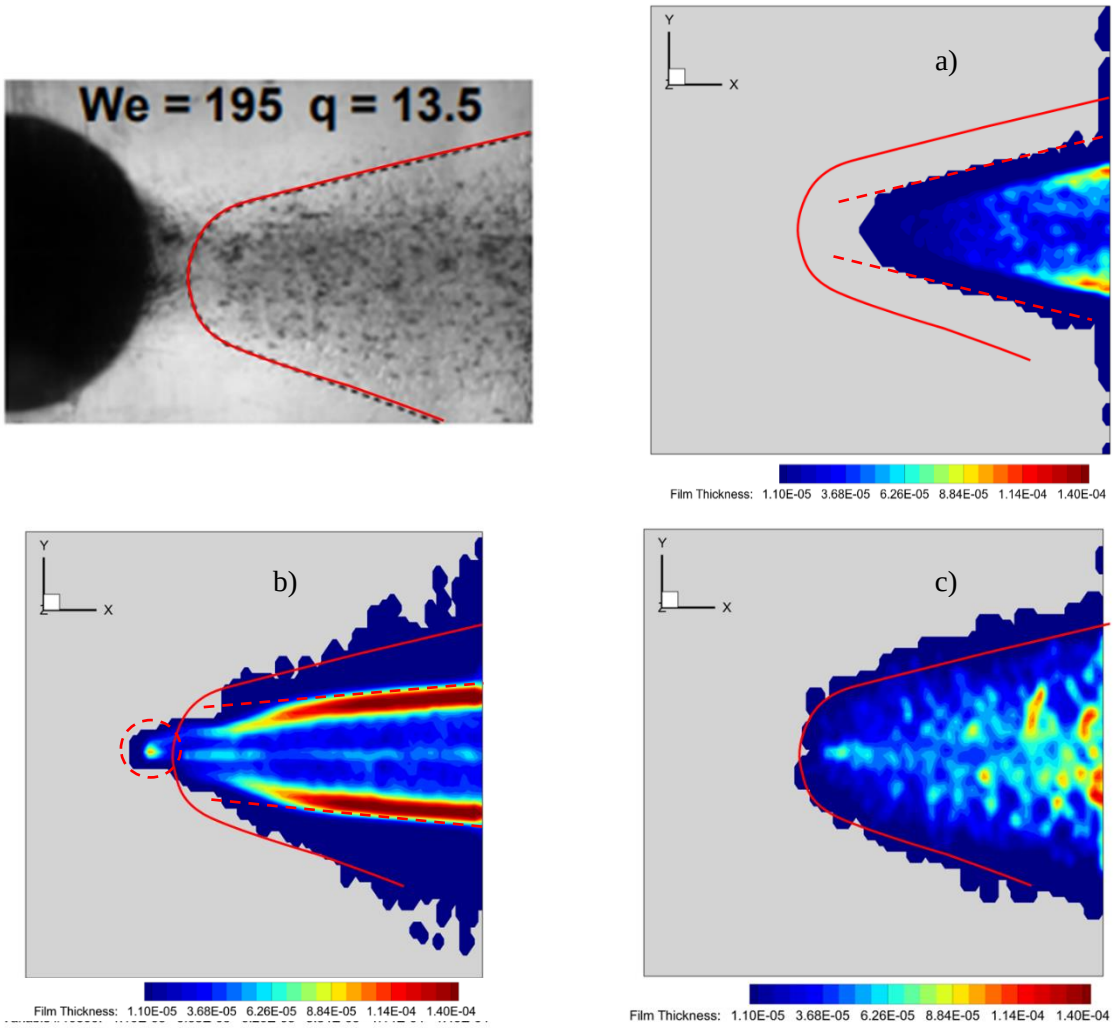

Figure 5: Qualitative comparison between experiments (top-left, [27]), and numerical results (shape coloured by film thickness): a) EWF-1way, b) EWF-2way, c) LWF-2way coupling.

Figure 5 shows the wall film shape and thickness obtained with the different approaches in comparison with the experiments. Figure 5-top-left reports a view of the experiments in [27] and [28], where the authors highlighted the wall film border (red line here), which is a triangle-like shape. The same border is then reported in the three simulations in the same position (Figure 5-a, -b, -c). As shown, film border in all the three simulations has a triangular shape but some differences can be noticed. In the EWF-1way (Figure 5-a), the generated film is very similar to the experiments (similar angular opening, red-dashed lines), but the film starting point is shifted forward in the streamwise direction. This behaviour was already explained by commenting Figure 4. In the EWF-2way case (Figure 5-b), the shape is still triangular with a similar angular opening (even if a more jagged border is observed), but focusing on the core of the wall film it is clear that the angular open is smaller (red-dashed line). Another point to notice is that in this case a displacement of the film is predicted before the red line limiting the film shape (red-dashed ellipse), which is not visible in experiments. The reason of such behaviour is still under investigation. LWF-2way (Figure 5-c) provides the film shape closest to the experiments, both for the film

borders and core. By comparing Figure 5-a, -b and -c, some other observations are observed. In fact, in the EWF simulations, a moustache shape is detected with larger film thickness near the film borders in EWF simulations (Figure 5-a, -b). On the contrary, in LWF simulation (Figure 5-c) the film mass is more evenly distributed along the spanwise direction, showing peaks in the maximum thickness closer to the centreline, as also showed by experiments. In general, from a qualitative viewpoint it is possible to conclude that LWF-2way approach better reproduces the experimental photogram showing a stronger agreement with the film shape and thickness distribution.

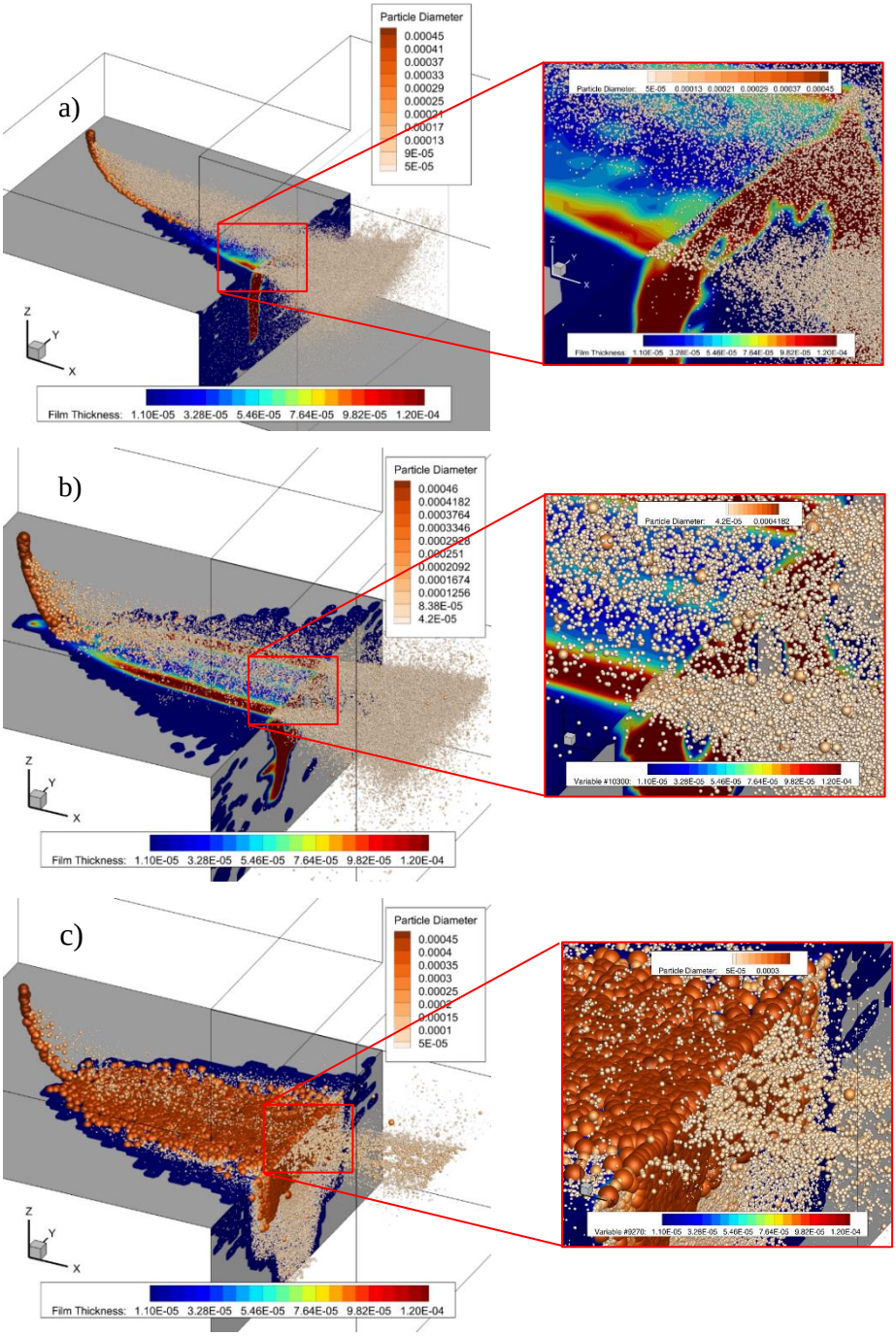

Figure 6: Screenshots of the disperse phase field and wall film thickness contour plot of the three simulations performed: a) EWF-1way; b) EWF-2way; c) LWF-2way coupling.

An overview of the disperse phase field (and liquid film shape) is presented in Figure 6: particle sizes in the figure are proportional to the real particle diameters by means of a scaling factor equals to 2. First of all, the difference in EWF and LWF approaches is evident: while the former (Figure 6-a, -b) tracks only the droplets entrained by the flow and separated from the trailing edge, the latter (Figure 6-c) tracks also liquid film particles deposited on the target surface. Water separation from the trailing edge of the target surface is shown in the three blow-ups in Figure 6. As explained in Section 2.2, separation occurs when a critical angle and a critical film Weber number are overcome. Since in the present simulation the geometry is the same in all the simulations, the detachment of liquid particles depends on film thickness and on the film velocity. As already noticed, in EWF simulations a characteristic moustache shape is detected with higher values of film thickness near the film borders. In these simulations, major separation phenomena are observed in these regions. On the other side, in LWF approach, the film thickness is larger close to the centre of the wet region, so droplet separation is mainly concentrated on the surface central region.

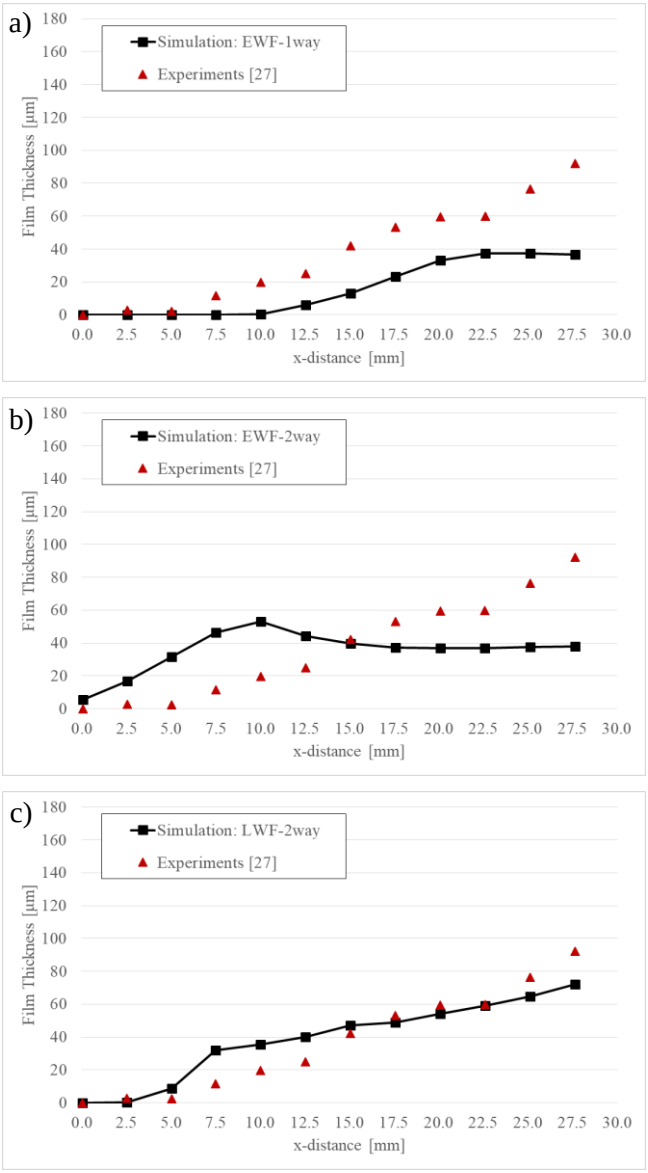

Figure 7: Comparison between experimental data (triangles) and sampled numerical results (black lines and squares) along the film centreline: a) EWF 1-way; b) EWF 2-way; c) LWF 2-way.

In Figure 7, a quantitative comparison of water film thickness on the centreline between the different numerical approaches and experiments is presented. The plots are obtained by computing, at each *x*-coordinate, the mean values of the wall film evolution in a period time as illustrated in Figure 3. The EWF-1way (Figure 7-a) model, tends to underestimate the film thickness but a similar trend is observed when results are compared with the experimental ones up to x=23 mm. In the last portion of the plate centreline, the wall film thickness is not well reproduced. On the contrary, EWF-2way results (Figure 7-b) show a very bad agreement with the experiments, overestimating the film thickness when x ranges in 0-13 mm and underestimating for x>15 mm. The LWF-2way (Figure 7-c) simulation provides the best results, from both a qualitative and a quantitative point of view. These results are summarized in Table 3 where average and maximum deviations between simulations and experimental measurements are reported. While the average deviation between numerical and experimental results is always higher than 20 μm for the Eulerian-based simulations (with maximum deviation values larger than 50 μm), in the LWF-2way simulation the average absolute error detected is 8.94 μm with a peak of 20.27 μm. In general, the numerical results show the maximum errors close to the impact point and to the wall edge. A major effort is probably needed to properly tune the injection/atomization model and the separation one.

Table 3: Deviations summary between experimental and computed film thickness values (x_{MD}: *x*-coordinate values of the maximum deviation).

Simulation	x_{MD} [mm]	Maximum Deviation [μm]	Average Deviation [μm]
EWF-1way	27.64	55.50	21.41
EWF-2way	27.64	53.98	24.43
LWF-2way	7.49	20.27	8.94

5. Conclusions

In the present paper we performed a series of numerical simulation of the liquid film formation on a horizontal flat surface. A liquid jet is crossflow-atomized in a rectangular channel and some droplets impinge on the opposite surface to the injection orifice, forming a thin film on the wall. The test case, because of the number of involved physical phenomena, was extensively used in literature to tune and validate numerical models. In the present work, the aim was to assess the different models implemented in ANSYS Fluent and to measure the accuracy of the simulations. Three different numerical approaches have been used to solve the film evolution, namely Eulerian one-way coupling, Eulerian two-way coupling and Lagrangian two-way coupling. While Eulerian approaches had already been validated on this case, the Lagrangian approach was just recently added in the commercial software and, to the authors' knowledge, was never used to reproduce such a complex test case. Moreover, in all the simulations, liquid column primary and secondary atomization, droplets-wall interaction and droplets separation from the liquid film at trailing edges, are considered by activating proper models. Results have been compared with experiments both qualitatively and quantitatively.

The simulation in which a Lagrangian two-way coupling approach was adopted to solve the liquid film dynamics on the target solid surface, is demonstrated to show the best results in comparison with experimental measurements, both from a qualitative and quantitative viewpoint. Indeed, in this case the wall film shape is very close to the experimental one, showing the same angular opening and similar distribution of the water mass. As detected also in the reference experiments, thickness peaks are concentrated in the central region of the wall film, while by using Eulerian approaches (both one- and two-way coupling) peaks are shifted to the lateral borders of the liquid film. A quantitative analysis is also performed by comparing the film thickness variation on the wall centreline. While the average deviation between numerical and experimental results is always higher than 20 μm for the Eulerian-based simulations (with

maximum deviation values larger than 50 μm), in the LWF-2way simulation the average absolute error detected is 8.94 μm with a peak of 20.27 μm.
In conclusion, among all the tested approaches, the Lagrangian two-way wall film model provides the best results. However, some more analyses need to be conducted to better understand what the discrepancies with the experiments are due to, with a focus on the injection/atomization model and to the separation modelling approach which are believed to play an important role in the overall physical observed behaviour. Once a full control on all the adopted sub-models will be reached, the approach will be mature to study more complex applications, as the occurrence of liquid wall film formation in compressors subject to water washing.

References

[1] United Nations. Paris Agreement. Paris climate change conference (COP21), Paris, France, 30 November to 12 December, 2015.
[2] Meher-Homji, C. B., Chaker, M. A. and Motiwala, H. M., Gas Turbine Performance Deterioration, Proceedings of 30th Turbomachinery Symposium, Houston, Texas, pp. 139-175, 2001.
[3] Aker, G.F., Saravanamuttoo, H.I.H., Predicting gas turbine performance degradation due to compressor fouling using computer simulation technique, Journal of Engineering for Gas Turbines and Power, vol. 111, pp. 343-350 (1989).
[4] Brooks, F.J., GE gas turbine performance characteristics, GE Power Systems, Report GER-3567H (2000).
[5] N. Aretakis, I. Roumeliotis, G. Doumouras, K. Mathioudakis, 2012, Compressor washing economic analysis and optimization for power generation, Applied Energy, vol. 95, 77-86.
[6] J.P. Stalder, Gas Turbine Compressor Washing State of the Art: Field Experiences, J. Eng. Gas Turbines Power, 123(2), pp. 363-370, 2001.
[7] Meher-Homji C. B., Broomley A., 2004, Gas turbine axial compressor fouling and washing, Proceedings of the 33rd turbomachinery symposium.
[8] S. Madsen, L.E. Bakken, 2018, Gas turbine fouling off-shore; effective online water wash through high water-to-air ratio, Proceedings of the ASME Turbo Expo 2018, June 11-15, Oslo, Norway, paper no. GT2018-75618, 2018.
[9] I. Dominizi, S. Gabriele, A. Serra, D. Borello, "Comparative Life Cycle Assessment of different Gas Turbine Axial Compressor Water Washing Systems", Proceedings of the ASME Turbo Expo 2020, 2020.
[10] R. Agbadede, P. Pilidis, U.L. Igie, I. Allison, "Experimental and theoretical investigation of the influence of liquid droplet size on effectiveness of online compressor cleaning for industrial gas turbines, Journal of the Energy Institute, vol. 88, pp. 414-424, 2015.
[11] I.R. Baikov, A.M. Suleimanov, M.I. Kuznetsova, S.V. Ki-taev, and Yu.V. Kolotilov, "Improvement of the Composition of Detergent Solutions for the Removal of Deposits on the Axial-Compressor Blades of Gas-Turbine Units", in Polymer Science, Series D, Vol. 11(1), pp. 82–85, 2018.
[12] L. Wang, Z. Yan, F. Long, X. Shi, J. Tang, "Parametric study of online aero-engine washing systems", International Conference on Aircraft Utility Systems, October 10-12,2016, Beijing, China, 2016.
[13] L. Wang, J. Hu, J. Huo, Q. Liu, B. Wei, J. Tang, X. Shi, "Study on the cleaning mechanism of the fouling of the compressor blade", CSAA/IET International Conference on Aircraft Utility Systems, Guiyang, China, 2018.
[14] U. Igie, P. Diez-Gonzalez, A. Giraud, O. Minervino, "Evaluating Gas Turbine Performance Using Machine-Generated Data: Quantifying Degradation and Impacts of Compressor Washing", ASME. J. Engineering for Gas Turbines Power, vol. 138(12), 2016.
[15] G. Musa, U. Igie, P. Pilidis, S. Gowon, "Economic Viability of On-Line Compressor Washing for Different Rated Capacity", in Proceedings of the ASME Turbo Expo 2017, Charlotte, North Carolina, USA. June 26–30, 2017.

[16] H. Margolis, 1991, U.S. Navy on-line compressor washing of marine gas turbine engines gas turbine engines, Proceedings of the International Gas turbine and Aeroengine Congress and Exposition, Oralndo, Florida, paper no. 91-GT-309.
[17] M. Wall, R. Lee e S. Frost, Offshore gas turbines (and major driven equipment) integrity and inspection guidance notes, Research Report 430 prepared by ESR Technology Ltd for the Health and Safety Executive, 2006.
[18] P. Venturini, M. Andreoli, D. Borello and F. Rispoli, S. Gabriele, "Modelling of water droplets erosion on a subsonic compressor cascade", Flow, Turbulence and Combustion, vol. 103(4); pp.1109-1125, 2019.
[19] F. Di Gruttola, G. Agati, P. Venturini, D. Borello, F. Rispoli, S. Gabriele, D. Simone, "Numerical study of erosion due to online water washing in axial flow compressors", Proceedings of ASME Turbo Expo 2020, Turbomachinery Technical Conference and Exposition, 2020.
[20] G. Agati, F. Di Gruttola, S. Gabriele, D. Simone, P. Venturini, D. Borello, "Water washing of axial flow compressors: numerical study on the fate of injected droplets", E3S Web Conf. Volume 197, 2020, 75th National ATI Congress – #7 Clean Energy for all (ATI 2020), 2020.
[21] G. Agati, F. Di Gruttola, S. Gabriele, D. Simone, P. Venturini, D. Borello, "Evaluation of water washing efficiency and erosion risk in an axial compressor for different water injection conditions", E3S Web Conf. Volume 312, 76th Italian National Congress ATI (ATI 2021), 2021.
[22] G. Agati, A. Castrorrini, F. Di Gruttola, S. Gabriele, F, Rispoli, D. Simone, P. Venturini, D. Borello, "Numerical prediction of long term droplet erosion and washing efficiency of an axial compressors through the use of a discrete mesh morphing approach", Proceedings of ASME Turbo Expo 2022, Turbomachinery Technical Conference and Exposition, 2022.
[23] Kim, M., & Min, K. (2002). Calculation of fuel spray impingement and fuel film formation in an HSDI diesel engine. KSME international journal, 16(3), 376-385.
[24] Senda, J., Kanda, T., Al-Roub, M., Farrell, P. V., Fukami, T., & Fujimoto, H. (1997). Modeling spray impingement considering fuel film formation on the wall. SAE transactions, 98-112.
[25] O'Rourke, P. J., & Amsden, A. A. (2000). A spray/wall interaction submodel for the KIVA-3 wall film model. SAE transactions, 281-298.
[26] Singh, K., Sharabi, M., Jefferson-Loveday, R., Ambrose, S., Eastwick, C., Cao, J., & Jacobs, A. (2021). Modeling of Partially Wetting Liquid Film Using an Enhanced Thin Film Model for Aero-Engine Bearing Chamber Applications. Journal of Engineering for Gas Turbines and Power, 143(4).
[27] Shedd, T., Corn, M., Cohen, J., Arienti, M., & Soteriou, M. (2009). Liquid film formation by an impinging jet in a high-velocity air stream. In 47th AIAA Aerospace Sciences Meeting including The New Horizons Forum and Aerospace Exposition (p. 998).
[28] Arienti, M., Wang, L., Corn, M., Li, X., Soteriou, M. C., Shedd, T. A., and Herrmann, M. "Modeling Wall Film Formation and Breakup Using an Integrated Interface-Tracking/Discrete-Phase Approach." ASME. J. Eng. Gas Turbines Power. March 2011; 133(3), 2010.
[29] Hee, J.L., Simmons, K., Kakimpa, B., & Hann, D., "Computationally Efficient Modelling of Oil Jet-Breakup and Film Formation for Bearing Chamber Applications." Proceedings of the ASME Turbo Expo 2018: Turbomachinery Technical Conference and Exposition. Volume 2C: Turbomachinery. Oslo, Norway. June 11–15, 2018.
[30] Nicoli, A., Jefferson-Loveday, R., & Simmons, K. "A New OpenFOAM Solver Capable of Modelling Oil Jet-Breakup and Subsequent Film Formation for Bearing Chamber Applications." Proceedings of the ASME Turbo Expo 2019: Turbomachinery Technical Conference and Exposition. Volume 2C: Turbomachinery. Phoenix, Arizona, USA. June 17–21, 2019.
[31] Meredith K V, Heather A, De Vries J and Xin Y 2011 A numerical model for partially-wetted flow of thin liquid films Computational Methods in Multiphase Flow VI 70 239
[32] Friedrich, M. A., Lan, H., Wegener, J. L., Drallmeier, J. A., & Armaly, B. F. (2008). A separation criterion with experimental validation for shear-driven films in separated flows. Journal of Fluids Engineering, 130(5).

[33] P. J. O'Rourke and A. A. Amsden. "A Particle Numerical Model for Wall Film Dynamics in Port-Fuel Injected Engines". SAE Paper 961961. 1996

[34] ANSYS Fluent Theory Guide, release 2021 R2. ANSYS, Inc., Southpointe, 2021.

[35] B. E. Launder and D. B. Spalding. "The Numerical Computation of Turbulent Flows", Computer Methods in Applied Mechanics and Engineering. 3. 269–289, 1974.

[36] Stanton, D.W. and C. J. Rutland, C.J., "Multi-Dimensional Modeling of Thin Liquid Films and Spray-Wall Interactions Resulting from Impinging Sprays", International Journal of Heat and Mass Transfer, Vol. 41, pp3037–3054, 1998.

[37] R. D. Reitz. "Mechanisms of Atomization Processes in High-Pressure Vaporizing Sprays". Atomization and Spray Technology, 3, 309–337, 1987.

[38] M. Pilch and C. A. Erdman. "Discrete Element Method (DEM) Simulation and Processing of Mo/AL2O3 Granules in Fluidizing Bed". Proc. Nat. Sci. Counc. RAOC(A). 24. 5. 394-404, 2000.

.